Artículo de Investigación. Revista Ciencia e Ingeniería. Vol. 47, No.2 pp. 153-164, abril-julio, 2026.
ISSN 1316-7081. ISSN Elect. 2244-8780 Universidad de los Andes (ULA)

Synthesis of activated carbons from natural sources for the removal of trace methane in specialized environments

Síntesis de carbones activados a partir de fuentes naturales para la eliminación de trazas de metano en ambientes especiales.

Lugo, Claudio[1]*; Marín Astorga, Karina[1†]; Pérez, Patricia[2]; Vizcaya, Marietta[2]; Rondón, Jairo[3]; Rodríguez, Pedro[1]

[1]Laboratorio de Cinética y Catálisis, Departamento de Química, Facultad de Ciencias, Universidad de Los Andes, Mérida, Venezuela.
[2]Laboratorio de Polímeros, Departamento de Química, Facultad de Ciencias, Universidad de Los Andes, Mérida, Venezuela.
[3]Biomedical Engineering Department, Universidad Politécnica de Puerto Rico, San Juan, Puerto Rico, USA.

**claudiolugo@ula.ve*

Abstract

Activated carbons (ACs) were synthesized from natural precursors (coconut shells and peach pits) via carbonization in a muffle furnace at 700 °C, followed by activation with nitric acid (HNO_3). The materials were characterized using Fourier Transform Infrared Spectroscopy (FTIR), X-ray Diffraction (XRD), Scanning Electron Microscopy (SEM), and Brunauer–Emmett–Teller (BET) analysis to determine the specific surface area (N_2 physisorption). XRD patterns revealed a highly disordered and/or amorphous structure, in which carbon layers are interconnected and intertwined, forming voids associated with porosity. BET surface area analysis showed that nitrogen adsorption increased after nitric acid activation; in all cases, Type I isotherms were observed according to the BDDT classification. SEM analysis indicated that non-activated coconut shell particles were smaller compared to those derived from peach pits. Finally, the CH_4 adsorption capacity of both non-activated and activated carbons was evaluated, showing that nitric acid–activated carbons exhibit enhanced adsorption capacity at low temperatures (40 °C).

Keywords: *Activated carbons, methane, greenhouse gases.*

Resumen

Se sintetizaron Carbones Activados (CAs) a partir del método de carbonización de la materia prima (cáscaras de coco y semillas de durazno) en una mufla a 700 °C y activación con ácido nítrico (HNO_3). Estos materiales se caracterizaron a partir distintas técnicas como la Espectroscopia infrarroja con transformada de Fourier, FTIR, la Difracción de rayos x, DRX, la Microscopia Electrónica de Barrido (MEB) y por Analizador B.E.T. para determinar el Área superficial (adsorción física de N_2). Los DRX obtenidos de las muestras presentan una estructura altamente desordenada y/o amorfa en las cuales las láminas de carbón se conectan y se entrelazan unas con otras, con espacios vacíos que corresponden a la porosidad. En los análisis de área superficial BET, las isotermas muestran que la cantidad adsorbida de nitrógeno es mayor después que el carbón es activado con ácido nítrico, en todos los casos se observó isotermas del tipo I de la clasificación de B.D.D.T. En el análisis por MEB se determinó que las partículas de las cáscaras de coco sin activar son de menor tamaño, respecto a los carbones de las semillas de duraznos. Finalmente se estudió la capacidad de adsorción de CH_4 de los carbones sin activar y activados, lo cual dio como resultado que los carbones activados con ácido nítrico presentan una mejor capacidad de adsorción a bajas temperaturas (40 ºC).

Palabras clave*: Carbones activados, metano, gases de invernadero.*

1 Introducción

Activated carbon is an amorphous form of carbon with a microcrystalline structure like graphite. This broad definition encompasses a wide variety of materials with diverse properties and applications (Mattson et al., 1971).

Under the term activated carbon, a range of products is grouped that differ in physical properties and composition; however, they all share a high degree of porosity and, therefore, a high adsorption capacity, with carbon as their main constituent. The term "activated" refers to the development of extensive porosity and specific surface area associated with the activation process, which ultimately determines the final characteristics of the material. Due to their high adsorption capacity, these carbons are widely used as adsorbents for various substances in both liquid and solid phases (Da Costa et al., 2015).

Adsorption is the change in concentration of a component at the surface of an adsorbent. The most relevant aspects of adsorption phenomena include (Parida, 2006): (i) interfacial characteristics, where adsorption represents the enrichment (positive adsorption) or depletion (negative adsorption) of one or more components at a surface; (ii) adsorption isotherms, which describe the mathematical relationship between the mass of adsorbed solute and its equilibrium concentration in solution; (iii) adsorption thermodynamics, based on equilibrium concepts and the Gibbs dividing surface model; and (iv) adsorbate–adsorbent interactions, which may be physical or chemical. Physical adsorption arises from weak interactions, such as van der Waals forces, and is associated with adsorption heats typically below 80 kJ/mol.

For adsorption processes, materials of greatest interest are those with high surface area, such as microporous and mesoporous solids, or materials combining micro-, meso-, and macroporosity, as in activated carbons (Haynes, 1988; Armatas et al., 2005; Ferreira et al., 2006). Industrial adsorbents and some activated carbons can reach surface areas of 1000-1500 m²/g (Nijhuis et al., 1999; Araújo et al., 2008).

Activated carbon can be produced from carbonaceous materials (e.g., coconut shells or fruit seeds) that are pyrolyzed and subsequently subjected to physical or chemical activation processes (Yalcin et al., 2002). Depending on the intended industrial application, activated carbon may be commercialized as: (1) granular carbon, with lower surface area and smaller pore diameter due to the binders used, or (2) powdered carbon, with higher surface area and larger pore size. To be considered an effective adsorbent, activated carbon must meet certain criteria: (i) high surface area, (ii) microporous structure, and (iii) high reactivity. Typically, industrial activated carbons exhibit surface areas of 800–1500 m²/g.

Activated carbons are also commonly used as support for adsorbing hydrocarbons derived from industrial processes. In 2005, Lee et al. investigated the adsorption capacity of these materials by modifying synthesis conditions, demonstrating significant adsorption performance with carbon tetrachloride (CCl_4) and ammonia (NH_3) over a relative pressure (P/P_0) range of 10^{-4} to 0.8 (Lee et al., 2005).

Currently, novel methodologies allow precise control over porosity and surface chemistry in molecular sieves and advanced carbon materials for catalytic applications. These include carbon molecular sieves, activated carbons, activated carbon fibers, carbon nanotubes, and graphite nanofibers (Parida, 2006). However, the potential application of the adsorption properties of these carbonaceous materials remains insufficiently explored. Activated carbons exhibit unique surface properties compared to other adsorbents, due to their slightly polar or nonpolar surfaces. This characteristic provides several advantages: (a) they are the only commercial adsorbents capable of performing separation and purification processes without requiring moisture removal, such as in air purification; (b) they effectively adsorb a wide range of nonpolar and weakly polar organic molecules due to their extensive internal surface area and large pore volume; and (c) their adsorption heat or bonding strength is generally lower than that of other adsorbents, facilitating easier desorption and regeneration through simple thermal treatment.

In processes involving mixtures of humid gases or aqueous solutions, the use of activated carbons is essential, as adsorption of nonpolar or weakly polar organic compounds is stronger under these conditions.

In this work, activated carbons were synthesized via carbonization, followed by chemical activation using concentrated nitric acid (HNO_3). The carbonaceous materials were characterized using Fourier Transform Infrared Spectroscopy (FTIR), X-ray Diffraction (XRD), Scanning Electron Microscopy (SEM), and BET surface area analysis. Adsorption tests were performed using a gas chromatograph (GC) coupled to the adsorption system to evaluate the adsorption capacity of the activated carbons toward greenhouse gases, particularly methane (CH_4).

2. Experimental Procedure

2.1 Synthesis of Activated Carbons

Activated carbons (ACs) were prepared from: (1) peach pits and (2) coconut shells using a modified impregnation method described by Kim and Ahn (Kim y Ahn, 2010) and validated at the Kinetics and Catalysis Laboratory of the Universidad de Los Andes by Marín (Marín, 2015) and Prado (Prado, 2018). This synthesis consists of two main stages:

2.1.1 Preparation of Carbonaceous Materials

The raw materials (peach pits and coconut shells) were treated via a carbonization process (Kim and Ahn, 2010), which allowed the production of the desired carbon materials.

2.1.1.1 Carbons from Peach Pits

Initially, the collected peach pit samples were washed with distilled water to remove pulp residues. They were then dried in an oven at 100 °C for 5 h, followed by further drying at 200 °C for 12 h prior to thermal treatment.

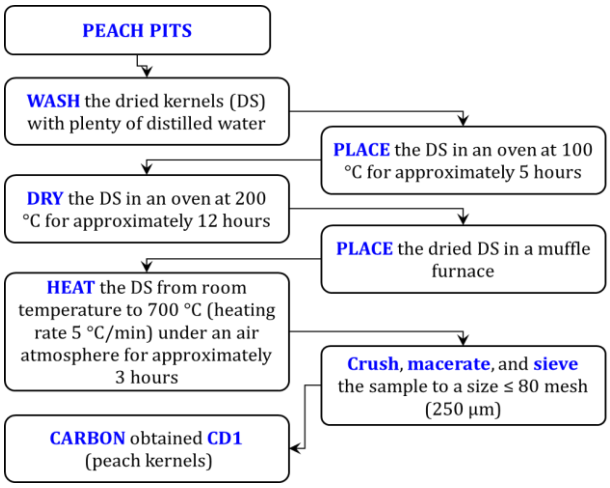

Fig. 1. Scheme of synthesis of Carbon obtained (CD1) from Peach seeds.

The carbonization process was carried out in a muffle furnace (with precise control of temperature ramp and time). The dried samples (~6.0 ± 0.1 kg) were heated from room temperature to 700 °C at a heating rate of 5 °C/min under an air atmosphere and maintained at 700 °C for approximately 3 h. The resulting solid (492.1 ± 0.1 g) was ground, crushed, and sieved to obtain particles ≤ 80 mesh (250 µm) (Kim and Ahn, 2010). The synthesis scheme is shown in Fig. 1.

2.1.1.2 Carbons from Coconut Shells

The collected coconut shells were sanded, washed, and boiled in distilled water at 100 °C for 5 h to remove residual organic matter. The cleaned shells were then dried at 200 °C for 12 h prior to thermal treatment.

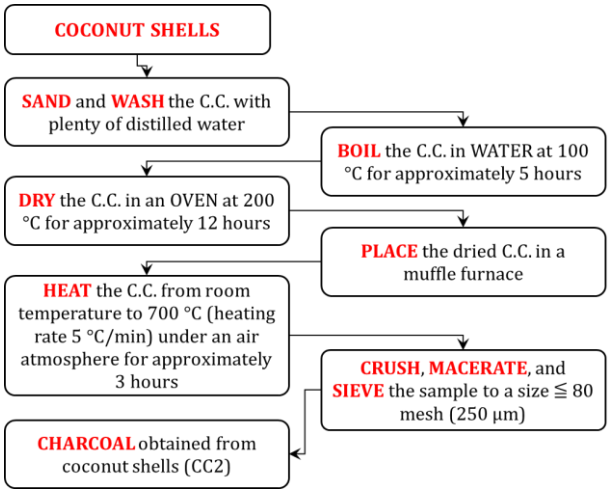

Fig. 2. Scheme of synthesis of Carbon obtained (CD1) from Coconut shells.

Carbonization was performed in a muffle furnace under controlled temperature and time conditions. The dried samples (~5.0 ± 0.1 kg) were heated from room temperature to 700 °C at 5 °C/min under an air atmosphere and held at 700 °C for approximately 3 h. The resulting solid (421.7 ± 0.1 g) was ground, crushed, and sieved to a particle size ≤ 80 mesh (250 µm) (Kim and Ahn, 2010). The synthesis scheme is shown in Figure 2.

2.1.2 Activation of Carbons

Chemical activation of the prepared carbons (from peach pits, CD1, and coconut shells, CC2) was carried out in a reflux system using nitric acid (HNO_3, 65 wt.%, Merck). First, ~400 mL of nitric acid was placed in a three-neck round-bottom flask. Subsequently, 4.0 g of carbon was slowly added under constant stirring (1000 rpm). The mixture was maintained at 75 °C under reflux for 16 h.

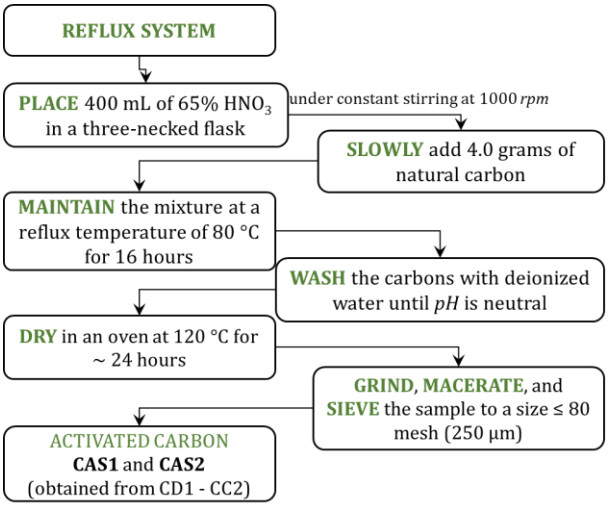

Fig. 3. Activation scheme of Activated Carbons (CAD1 and CAC2).

After chemical activation, the resulting activated carbons were washed with abundant deionized water until the pH reached neutrality. Finally, the activated carbons (CAD1 and CAC2) were dried in an oven at 120 °C for 24 h. The procedure is illustrated in Fig. 3.

2.2 Synthesized Materials

The activated carbons obtained from different natural sources (peach pits (SD1) and coconut shells (CC2)) are summarized in Table 1.

Table 1. Activated Carbons from different types of raw materials (SD1 and CC2) synthesized via SCS.

Material	Method	Code
Carbon (SD)	Impregnation	CD1
Carbon (CC)	Impregnation	CC2
Activated carbon (SD)	—	CAs1
Activated carbon (CC)	—	CAs2

SD: peach pits; CC: coconut shells

2.3 Characterization

The synthesized materials were characterized using the following techniques:

1. **Fourier Transform Infrared Spectroscopy (FTIR)** using a PerkinElmer Frontier spectrophotometer (Kinetics and Catalysis Laboratory, Universidad de Los Andes).
2. **X-ray Diffraction (XRD)** (powder method) using a Rigaku Geiger flex diffractometer (Metal Catalysis Laboratory, Universidad de Concepción, Chile), employing Cu Kα radiation at 40 kV and 2 mA. Operating conditions included continuous scan mode at 1°/min over a 2θ range of 1–90°.
3. **Scanning Electron Microscopy (SEM)** using a JEOL JEM 100-CX II microscope (Universidad de Concepción, Chile).
4. **BET Surface Area Analysis** using a Micromeritics ASAP 2020 analyzer (Johnson Matthey Inc., Sevierville, TN, USA) to determine specific surface area via N_2 physisorption.

All analyses were performed on both activated and non-activated samples.

3. Results and Discussion

3.1 Fourier Transform Infrared Spectroscopy (FTIR)

The infrared spectra of non-activated carbons obtained from peach pits and coconut shells (CD1–CC2) are shown in Fig. 4. Table 2 summarizes the FTIR band assignments for the non-activated carbons.

The broad band observed in the range 3700–3300 cm^{-1} is attributed to O–H stretching vibrations, indicating the presence of moisture in the synthesized samples (non-activated carbons) (Primera et al., 2011). Peaks between 2925.2 and 2856 cm^{-1} correspond to symmetric and asymmetric stretching vibrations of aliphatic C–H bonds (–CH_3 and –CH_2) (Rosquete, n.d.).

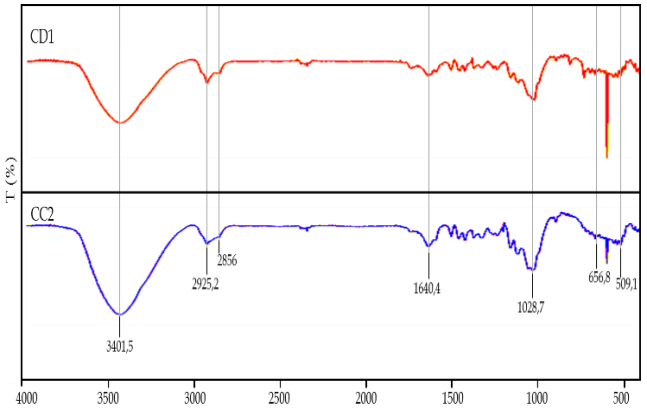

Fig. 4. FTIR spectra of non-activated carbons obtained from coconut shells (CC2) and peach pits (CD1).

The signal around 1640.4 cm^{-1} is associated with C=C stretching vibrations characteristic of aromatic compounds (Primera et al., 2011). Absorption bands near 959 cm^{-1} are attributed to in-plane bending vibrations of C–H bonds (Primera et al., 2011). Peaks around 656.8 cm^{-1} and 509.1 cm^{-1} correspond to out-of-plane bending vibrations of aromatic structures (Yin et al., 2009).

Table 2. FTIR band assignments for non-activated carbons synthesized from different raw materials (SD1 and CC2).

$\nu_{(ref.)}$ (cm^{-1})	ν (cm^{-1})	Bond	Assignment
3700–3300	3428.6	O–H	Symmetric and asymmetric O–H stretching
2950–2845	2925.2–2856	C–H	Symmetric and asymmetric stretching (aliphatic –CH_2 – CH_3)
1650–1600	1640.4	C=C	Aromatic C=C stretching
1440–880	1400–1028	C–H	In-plane bending vibrations
650	~656.8	H–C=C	Out-of-plane aromatic bending
455	~509.1	H–C=C	Out-of-plane aromatic bending

The FTIR spectra of activated carbons (CAs1–CAs2) are shown in Fig. 5, and their band assignments are presented in Table 3.

The broad band at ~3405 cm^{-1} corresponds to O–H stretching vibrations, indicating the presence of moisture in the activated samples (Primera et al., 2011). Weak bands between 2928 and 2855.5 cm^{-1} are associated with aliphatic C–H stretching vibrations (Rosquete, n.d.). The signal at ~1717.8 cm^{-1} is attributed to C=O stretching from functional groups such as ketones, aldehydes, lactones, or carboxylic acids (Rosquete, n.d.).

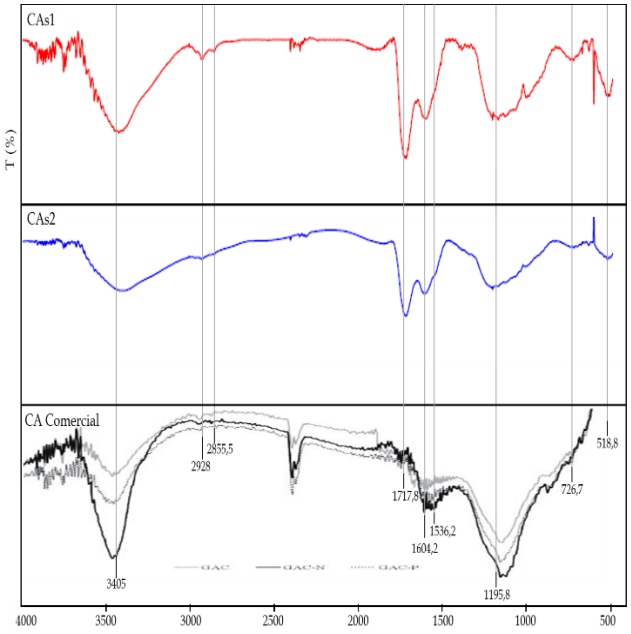

Fig. 5. FTIR spectra of activated carbons (HNO_3-treated) obtained from coconut shells (CAs2) and peach pits (CAs1).

Table 3. FTIR band assignments for activated carbons (CAs1 and CAs2).

$\nu_{(ref.)}$ (cm^{-1})	ν (cm^{-1})	Bond	Assignment
3700–3300	3405	O–H	Symmetric and asymmetric O–H stretching
2950–2845	2928–2855.5	C–H	Aliphatic C–H stretching
1765–1645	~1717.8	C=O	Carbonyl stretching (ketones, aldehydes, lactones, carboxylic acids)
1650–1600	1604.2–1536.2	C=C	Aromatic C=C stretching
1260–1180	~1195.8	C–O	Ester C–O stretching
790–650	~726.7	H–C=C	Out-of-plane aromatic bending
455	~518.8	H–C=C	Out-of-plane aromatic bending

Bands at 1604.2 and 1536.2 cm^{-1} correspond to aromatic C=C stretching vibrations (Primera et al., 2011). The peak at ~1195.8 cm^{-1} is assigned to C–O stretching in esters (Primera et al., 2011). Bands near 726.7 cm^{-1} and 518.8 cm^{-1} correspond to out-of-plane bending vibrations of aromatic structures (Yin et al., 2009).

3.2 X-ray Diffraction (XRD)

Figure 6 shows the diffraction patterns of non-activated (CD1–CC2) and activated carbons (CAs1–CAs2).

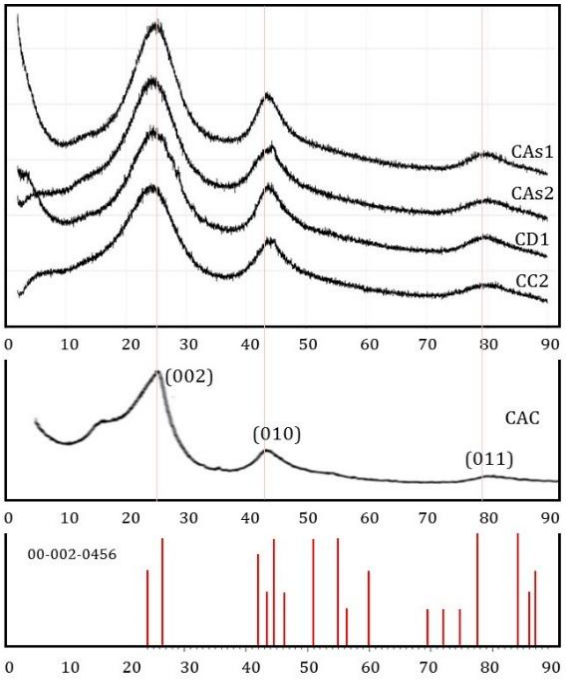

Fig. 6. XRD patterns of carbons obtained from peach pits and coconut shells (non-activated and activated). Activated carbon pyrolyzed at 800 ºC (Yin y col., 2009). File: 00-002-0456 (Graphite, carbon).

Phase identification was carried out using X'Pert HighScore Plus software with the PDF2-2004 ICDD database, revealing a hexagonal graphitic carbon phase (space group: *P63mc*), identified by card 01-088-0638 (Harcourt et al., 1942), and confirmed by comparison with literature (Yin et al., 2009; Liu et al., 2014).

The diffraction peaks correspond to the (002), (010), and (111) planes. The (002) reflection is associated with stacked aromatic layers, whereas the (010) and (111) reflections correspond to less ordered aromatic structures (Yin et al., 2009). Furthermore, the activated carbon synthesized in this study shows a diffraction pattern identical to that obtained for a commercial activated carbon studied by Liu et alia in 2014 (Liu et al., 2014).

The most intense peak near 25° is attributed to graphitic plate formation, indicating the development of a carbon–pore structure. Increasing the calcination temperature reduces the interlayer spacing and increases the crystallite size, promoting a transition from amorphous to semicrystalline carbon structures (Rampe et al., 2011).

3.3 Nitrogen Adsorption Isotherms

Figures 7 and 8 show nitrogen adsorption isotherms at 77 K for non-activated and activated carbons. Nitrogen adsorption increases after nitric acid activation, indicating enhanced micro- and mesoporosity.

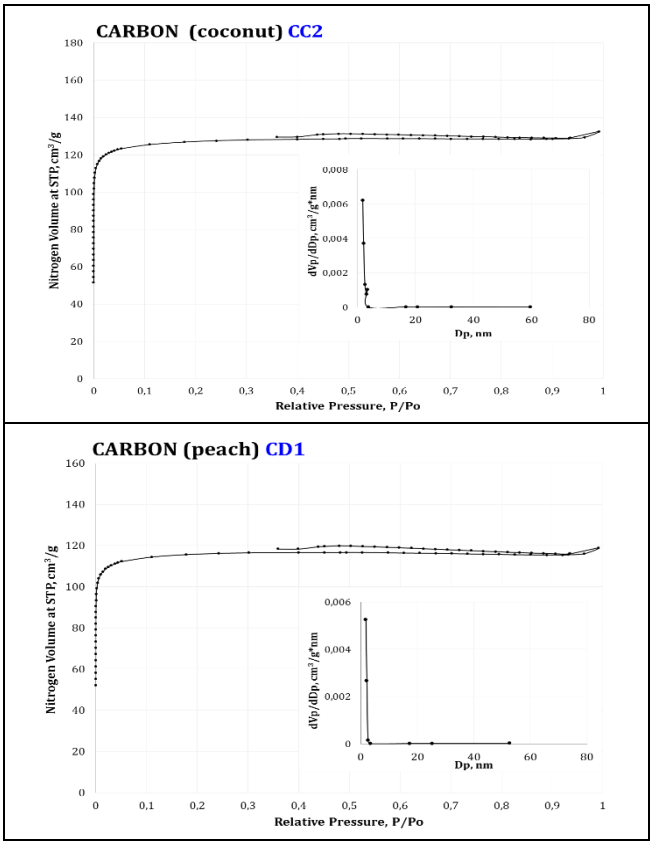

Fig. 7. N_2 adsorption isotherms (77 K) for non-activated carbons (CD1, CC2).

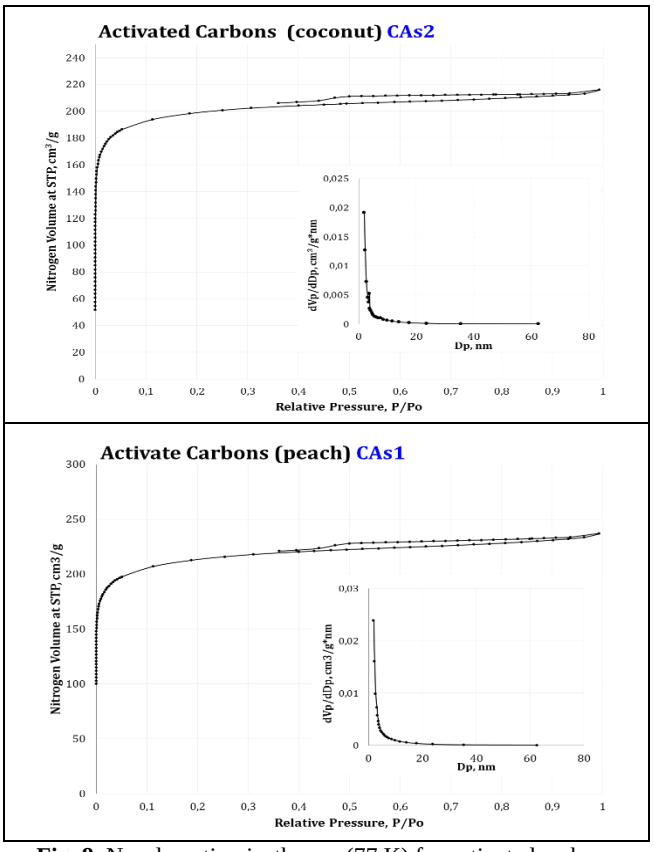

Fig. 8. N_2 adsorption isotherms (77 K) for activated carbons (CAs1, CAs2).

All samples exhibit Type I isotherms according to the Brunauer–Deming–Deming–Teller (BDDT) classification, confirming the predominance of microporosity.

Non-activated carbons show pore radii between 1 and 5 nm, while activated carbons exhibit increased pore diameters (~5–10 nm). BET results (Table 4) indicate increased surface area and pore volume after activation.

Table 4. Textural properties of synthesized carbons (from coconut shells and peach seeds).

Solid	Code	A_{BET} (m^2/g)	Report *t*-plot		V_{PORE}* (cm^3/g)	D_{PORE}* (nm)
			A_{MICRO} (m^2/g)	A_{EXT} (m^2/g)		
Carbon (coconut)	CC2	350 ± 2	326.0	21.0	0.18	4.42
Carbon (peach)	CD1	380 ± 2	343.7	36.2	0.20	4.62
Activated carbon (coconut)	CAs2	600 ± 3	-----	-----	0.33	3.81
Activated carbon (peach)	CAs1	694 ± 5	538.0	116.8	0.37	3.94

* *measured by BJH adsorption.*

3.4 Scanning Electron Microscopy (SEM)

SEM micrographs (Fig. 9) of non-activated carbons show heterogeneous particles (1–20 µm), irregular shapes, sharp edges, and cracks that contribute to surface area. Coconut-derived carbons exhibit higher heterogeneity than

peach-derived carbons.

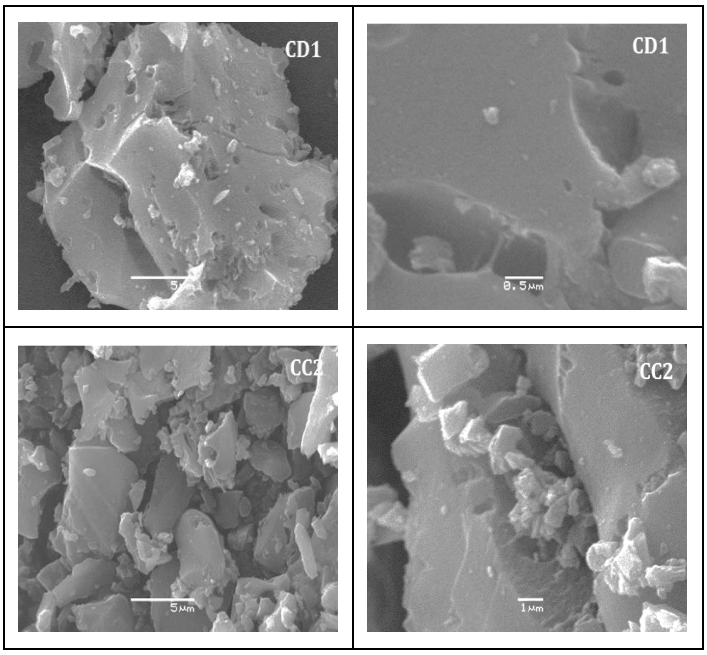

Fig. 9. SEM images of non-activated carbons (CD1, CC2).

After activation (Fig. 10), coconut carbons show minor morphological changes, while peach-derived carbons exhibit reduced particle size and increased surface roughness and porosity (36,2 to 116,8 m^2*g^{-1}).

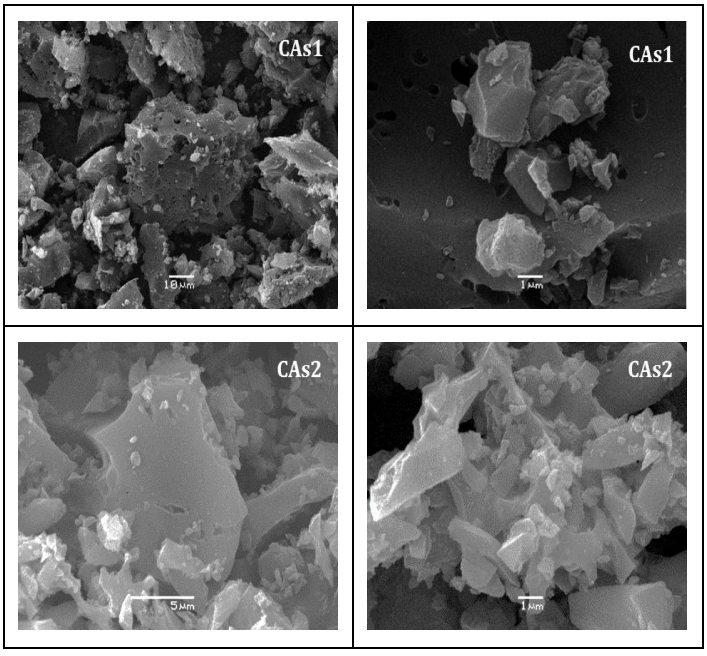

Fig. 10. SEM images of activated carbons (Cas1, CAs2).

In general, carbons obtained from coconut shells have fewer surface irregularities compared to carbons obtained from peach seeds; in addition, chemical treatment allows for a decrease in the particle size of peach seed carbons, leading to a more pronounced increase in the surface area of peach seed carbons than in the case of coconut shells.

3.5 Methane Adsorption Tests

3.5.1 Instrumental Response

A Hewlett-Packard 6890 Plus gas chromatograph equipped with a thermal conductivity detector (TCD) was used, with nitrogen as carrier gas (30 *mL*/min).

3.5.2 Pretreatment

About 200 mg of activated carbon (from coconut or peach) was placed inside a U-shaped steel reactor and the solid was pretreated by circulating ~30 mL/min of gaseous nitrogen, N_2(g), through the reactor from room temperature to 120 ºC, where it remained for 90 minutes.

3.5.3 Calibration (CGases)

Parameters such as mass, hydrocarbon flow rate, temperature range, and space velocity were calibrated. The ideal conditions for studying methane adsorption on activated carbons are shown in Table 5 below.

3.5.4 Adsorption Conditions

After the sample pretreatment was completed, 103 mL/min of a CH_4/N_2 (3/100) mixture was passed through the reactor. The adsorbent (CAs) was subjected to a temperature ramp from room temperature to the adsorption temperature of 40°C and 60°C, where it remained for a little over 1 hour (~100 minutes). The adsorption scheme is shown in Figure 11.

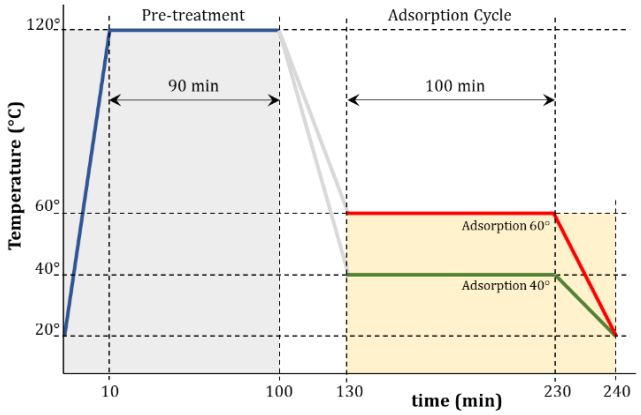

Fig. 11. Schematic of methane adsorption on activated carbons (coconut shells and peach seeds).

Table 5. Actual conditions for *CGases* analysis.

Parameter	Value
Total flow rate (*mL/min*)	~ 30
Temperature range (°C)	40-60
Activated carbon mass (*mg*)	≥ 0,030
Space velocity range x10^{-3} (*mL/g.h*)	120-240

3.5.5 Adsorption Tests of methane

Figure 12 (Table 6) shows the methane adsorption capacity during the studied cycle, which contains non-activated carbons (CC2-CD1) and activated carbons with nitric acid (CAs2-CAs1), prepared from different raw materials (coconut shells and peach pits), at temperatures between 60 and 40 °C. In this graph (Fig. 12), a linear behavior of methane (conductimetric response with respect to CGases) is observed before passing through the reactor, that is, at times below 25 minutes.

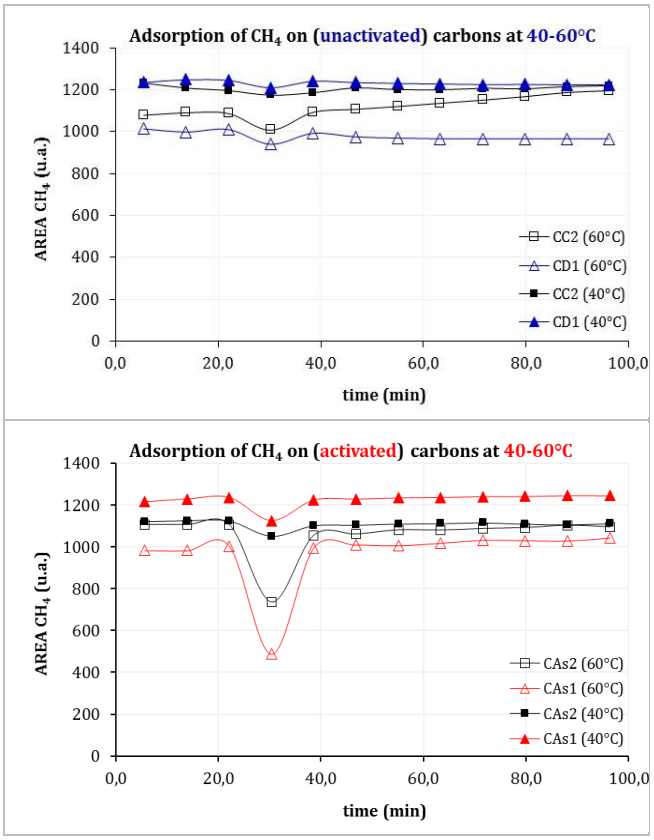

Fig. 12. Adsorption of methane on non-activated carbons (CC2 and CD1) and activated carbons (CAs2 and CAs1) at different temperatures, 40 and 60 °C.

Once the hydrocarbon enters the reactor, it can be determined that the amount of methane adsorbed onto

activated carbons (ACs) increases compared to non-activated carbons at different adsorption temperatures, 60 and 40°C. After the adsorbent is saturated, the initial methane concentration is recovered. This increase in the adsorptive capacity of activated carbons (ACs2-ACs1) compared to non-activated carbons (CC2-CD1) is due to the fact that the smaller the mesopore size and the height of the crosslinking of the polyaromatic molecules that compose it, the better the activation process, resulting in products with medium-sized pores; in addition, there is a significant increase in the porosity and volume of the micropores.

Table 6. Percentage Adsorption Data of methane on non-activated (CC2-CD1) and activated carbons (CAs2-CAs1) at 40 and 60 °C.

Adsorbent	time (min)	Area methane (u.a.)	Adsorption (%)
60 °C			
CAs2	30,4	735	**33,47**
CAs1	30,4	487	**50,79**
CC2	30,3	1010	**7,16**
CD1	30,2	940	**6,81**
40 °C			
CAs2	30,4	1052	**6,42**
CAs1	30,4	1126	**8,27**
CC2	30,3	1175	**3,04**
CD1	30,4	1210	**2,78**

These "new" properties give activated carbons a high degree of hydrocarbon adsorption (Martínez et al., 2013). Based on these results, it is possible to indicate that the adsorption capacity of activated carbons increases due to the modification of their surface, which, after activation, exhibits chemical species that change its acidity, making it more reactive to the molecules of the hydrocarbon studied (methane).

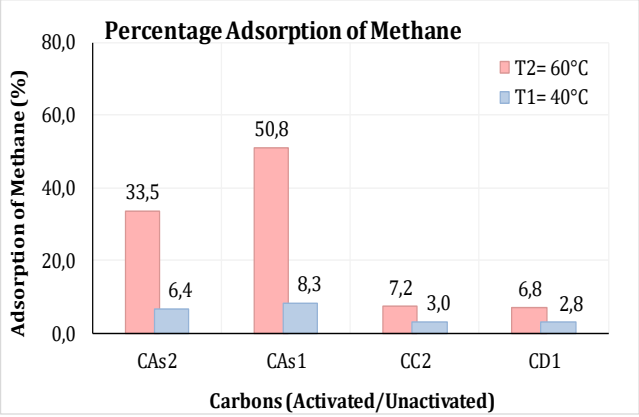

Fig. 13. Percentage Adsorption of methane on non-activated carbons (CC2-CD1) and activated carbons (CAs2-CAs1) at different temperatures 40 and 60 °C.

Due to 1) the nonpolar nature of activated carbons and 2) the type of forces involved in the different adsorption processes, they have the capacity to preferentially retain nonpolar molecules of high molecular weight (long-chain hydrocarbons, phenols, dyes, among others); while substances such as CH_4, CO_2, H_2, N_2, O_2, and H_2O are practically not retained by the carbon at room temperature.

This would explain the experimental results obtained: at 60 °C, the highest methane adsorption capacities are observed, with adsorption percentages between 33.5 and 50.8%, compared to the same activated carbons (CAs2-CAs1) tested at 40 °C, whose adsorption percentages are between 6.4 and 8.3 %, that is, below 10 % (Fig. 13, Table 6). Furthermore, the organic species studied (methane) that is expected to adsorb onto activated carbons has a low molecular weight and is highly diluted in high amounts of nitrogen (N_2/CH_4 100/3 mL); in this case, retention at room temperature by the carbon is only effective if it is impregnated with specific reagents or if the catalytic properties of the carbon are taken advantage of.

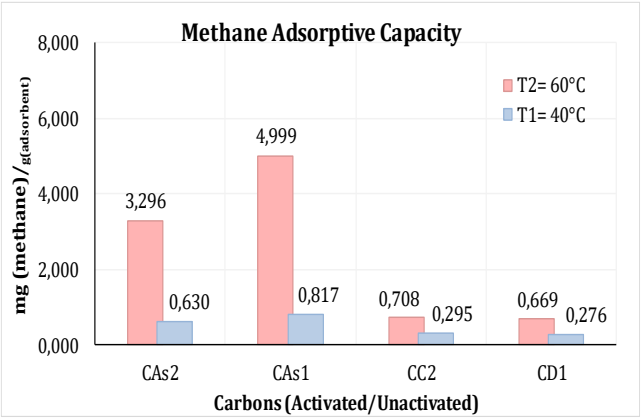

Fig. 14. Adsorptive Capacity of methane on non-activated carbons (CC2-CD1) and activated carbons (CAs2-CAs1) at different temperatures 40 and 60 °C.

Figure 14 shows the methane adsorption capacity for different activated (CAs2-CAs1) and non-activated (CC2-CD1) carbons at different working temperatures of 60 and 40 °C. In all cases, the interaction or adsorption force of the adsorbate (methane) with the surface of the adsorbent (carbonaceous species) is weak, favoring physisorption (Van Der Waals forces); in other words, high energies are not needed for the adsorption of the hydrocarbon to occur on the surface of the carbonaceous adsorbent (Droguett, 1983).

The activated carbon obtained from peach seeds, CAs1, at 60 °C (which showed the highest percentage adsorption of all the synthesized carbons 50.79%), shows an adsorptive capacity ~ 1,001 mg of CH_4 for every 1,968 mg of CH_4 injected into the total 103 *mL* that circulate through the system stream (Table 7).

Table 7. Adsorptive Capacity Data of methane on non-activated (CC2-CD1) and activated carbons (CAs2-CAs1) at 40 and 60 °C.

Adsorbent	ppm (CH_4) adsorbent	mg (CH_4) adsorbent	Cap. Adsorptive mg/g(adsorbent)
60°C			
CAs2	5188,40	0,659	3,296
CAs1	**7867,79**	**1,001**	**4,999**
CC2	1115,12	0,142	0,708
CD1	1053,13	0,134	0,669
40°C			
CAs2	991,22	0,126	0,630
CAs1	**1285,48**	**0,163**	**0,817**
CC2	464,63	0,059	0,295
CD1	433,66	0,055	0,276

grams $_{(adsorbent)}$ = 0,200
mg (CH_4) $_{(initials)}$ = 1,968

This allows us to determine that the adsorptive capacity of this solid is 4,999 mg of methane per 200 mg of initial adsorbent (~ 24,994 mg of methane per gram of activated carbon). A good CA-type adsorbent should have an adsorptive capacity between 20 and 50% of its own mass, which means that between 0.2 and 0.5 g of methane should be adsorbed per gram of activated carbon (Álvarez, 2016). The adsorption capacity for the other adsorbents is shown in Table 7.

Conclusions

Fourier Transform Infrared (FTIR) spectroscopy revealed the characteristic bands of carbonaceous materials and their transformation after treatment with nitric acid. The infrared spectra of the activated carbons exhibit typical functional groups of carbon materials, along with nitrate-related species that remain after washing the carbonized product with deionized water.

X-ray diffraction (XRD) patterns showed broad diffraction peaks, indicating the predominantly amorphous nature of the synthesized solids, with nanometric crystalline domains ($\lesssim$ 100 nm). A predominant hexagonal graphitic carbon phase (space group: $P6_3mc$) was identified using the PDF2-2004 ICDD database (card 01-088-0638) and confirmed through comparison with literature reports.

BET surface area analysis demonstrated that nitrogen adsorption increases significantly after activation with nitric acid. In all cases, Type I isotherms according to the Brunauer–Deming–Deming–Teller (BDDT) classification were observed, confirming the predominance of microporosity and relatively moderate surface areas. These results indicate that the synthesized materials contain a higher fraction of micropores compared to mesopores.

Textural analysis using SEM micrographs provided insight into the morphology of the prepared carbons. Non-activated coconut shell carbons exhibited smaller particle sizes compared to those derived from peach pits. The presence of cracks and openings in the peach pit-derived carbon (CD1) facilitates access to its internal structure, resulting in a higher surface area than in coconut-derived carbon (CC2), in agreement with BET results.

For activated carbon, the morphology of coconut-derived carbon (CAs2) showed minimal changes after nitric acid treatment, although a slight increase in particle dispersion was observed, thereby increasing surface area. In contrast, peach pit-derived activated carbon (CAs1) exhibited significant morphological changes, including reduced particle size and a pronounced increase in surface area, highlighting the stronger effect of HNO_3 activation.

Methane adsorption tests using gas chromatography demonstrated that nitric acid-activated carbons exhibit higher methane uptake compared to non-activated carbons, particularly at higher temperatures (60 °C vs. 40 °C). After saturation of the adsorbent, the initial methane concentration was recovered in all cases.

Temperature plays a crucial role in the adsorption process. At 60 °C, activated carbons showed the highest adsorption capacities, with methane adsorption percentages ranging from 6.8% to 50.8%, compared to values between 2.8% and 8.3% at 40 °C. The activated carbon derived from peach pits (CAs1) evaluated at 60 °C exhibited the highest adsorption capacity among all synthesized materials, reaching approximately 1.001 mg of CH_4 adsorbed per 1.968 mg of methane injected into the 103 mL gas stream.

4 References

Álvarez N., (**2016**), Capture from biogas streams adsorption processes for CO_2, Programa de Doctorado en Ingeniería Energética, Universidad de Oviedo, España, 50-51.

Araújo R., Azevedo D., Cavalcante C., Jiménez A., Rodríguez E., (**2008**), Adsorption properties of natural Cu(II), Zn(II) and Ag(I) exchanged Cuban mordenites, *Microporous and Mesoporous Materials*, Vol. 108 (1-3), pp. 213-222.

Armatas G., Petrakis D., Pomonis P., (**2005**), Estimation of diffusion parameters in functionalized silica's with modulated porosity: Part I: Chromatographic studies, *Journal of Chromatography Analysis*, Vol. 1074(1-2), pp. 53-59.

Da Costa A., De Carvalho S., Barros D., De Alcántara R., Oliveira M., (**2015**), Surface Modification of Commercial Activated Carbon (CAG) for the Adsorption of Benzene and Toluene, *American Journal of Analytical Chemistry*, Vol. 6(6), pp. 528-538.

Droguett S.E., (**1983**), *Elementos de Catálisis Heterogénea*, Serie de Química: Monografía, OEA. Programa Regional de Desarrollo Científico y Tecnológico,

Número 26 de Serie de química, Universidad de Texas, USA, 43-46.

Ferreira A., Mittelmeijer-Hazeleger M., Bliek A, (**2006**), Adsorption of normal and iso-butane on zeolite MFI, *Microporous and Mesoporous Materials*, Vol. 91(1-3), pp. 47-52.

Harcourt G.A., (**1942**), Tables for the identification of ore minerals by X-ray powder patterns, *The American Mineralogist*, Vol 27, 63-113.

Haynes H., (**1988**), The Experimental Evaluation of Catalyst Effective Diffusivity, *Catalysis Review Science Engineering*, Vol. 30(4), pp. 563-627.

Kim K-J., Ahn H-G., (**2010**), The adsorption and desorption characteristics of a binary component system of toluene and methylethylketone on activated carbon modified with phosphoric acid, *Carbon*, Vol. 48(8), pp. 2198-2202.

Lee W., Park J., Sok J., Reucroft P., (**2005**), Effects of pore structure and surface state on the adsorption properties of nano-porous carbon materials in low and high relative pressures, *Applied. Surface Science*, Vol. 246(1-3), pp. 77-81.

Liu B., Wang W., Wang N., Tong Au C., (**2014**), Preparation of activated carbon with high surface area for high-capacity methane storage, *Journal of Energy Chemistry*, vol. 23(5), pp.662-668.

Mattson J., Mark H., (**1971**), Activated Carbon: Surface Chemistry and Adsorption from Solution, Marcel Dekker, Inc New York, pp. 238-239.

Marín-Astorga† K., (**2015**), *Síntesis y caracterización de adsorbentes del tipo carbonáceos para trazas de metano*, Trabajo Especial de Grado (Lic. en Química), Laboratorio de Cinética y Catálisis, Departamento de Química, Facultad de Ciencias, Universidad de Los Andes, Mérida-Venezuela, pp. 1-84.

Martínez M., Molina M., Rodríguez F., (**2013**), *Preparación de carbones activados con KOH a partir de residuos de petróleo*. Adsorción de hidrógeno, Departamento de química inorgánica, Universidad de Alicante, España.

Nijhuis T., van den Broeke L., Linders M., van de Graaf J., Kapteijn F., Makkee M., Moulijn J., (**1999**), Measurement and modeling of the transient adsorption, desorption and diffusion processes in microporous materials, *Chemical Engineering Science*, Vol. 54(20), pp. 4423-4436.

Parida, S., (**2006**), Adsorption of organic molecules on silica surface Advances in Colloid and Interface, *Science*, Vol. 121, pp. 77-110.

Prado J., (**2018**), *Síntesis y caracterización de carbón activado obtenido a partir de residuos lignocelulósicos de la caña de azúcar, cáscara de coco y semillas de durazno y su empleo como adsorbente de CO_2, H_2 y CH_4*, Trabajo Especial de Grado (Lic. en Química), Laboratorio de Cinética y Catálisis, Departamento de Química, Facultad de Ciencias, Universidad de Los Andes, Mérida-Venezuela, pp. 1-122.

Primera O., Colpas F., Meza E., Fernández R., (**2011**), Carbones activados a partir de bagazo de caña de azúcar y zuro de maíz para la adsorción de cadmio y plomo. *Revista de la Academia colombiana de ciencias exactas físicas y naturales*, Vol. 35(136), 387-396.

Rampe J., Setiaji B., Trisunaryanti W., Triyono I., (**2011**), Fabrication and Characterization of carbon composite from coconut shell carbon, *Indian Journal Chemistry*, Vol. 11 (2), pp.124-130.

Rosquete C., S/A. Análisis orgánico (tablas). Laboratorio de Productos Naturales, Facultad de Ciencias, Departamento de química, Universidad de los Andes.

Yin Y., Zhang J., Sheng C., (**2009**), Effect of pyrolysis temperature on the char micro-structure and reactivity of NO reduction, *Korean Journal Chemistry Engineering*, Vol. 26(3), pp. 895-901.

Yalcin M., Arol A., (**2002**), Gold cyanide adsorption characteristics of activated carbon of non- coconut shell origin, *Hydrometallurgy*, Vol. 63(2), pp. 201-206.

Received: *november 22, 2025*

Accepted: *february 22,2026*

Lugo González, Claudio Antonio: *Ph.D. in Applied Chemistry, mention Materials Studies, 2017, Universidad de Los Andes; Professor of Chemistry Department (Kinetics and Catalysis Laboratory), at the Faculty of Sciences, ULA. Mérida, Venezuela.*

https://orcid.org/0000-0001-8003-0354

Marín Astorga, Karina†: *Bachelor's Degree in Chemistry, 2015, Chemistry Department (Kinetics and Catalysis Laboratory) at the Faculty of Sciences, Universidad de Los Andes, Mérida. karinasolangemarinastorga@gmail.com*

Pérez Dávila, Patricia: *Ph.D. in Drug Chemistry, 2017, Scientific Research Institute, Faculty of Pharmacy and Bioanalysis, Universidad de Los Andes; Professor of Polymer Laboratory at the Faculty of Sciences, ULA. Mérida, Venezuela. Email: perezdpatricia@gmail.com*

https://orcid.org/0000-0003-0591-2351

Vizcaya, Marietta: *Ph.D. in Drug Chemistry, 2014, Scientific Research Institute, Faculty of Pharmacy and Bioanalysis, Universidad de Los Andes; Professor of Polymer Laboratory at the Faculty of Sciences, ULA. Mérida, Venezuela. Email: marietta@ula.ve*

https://orcid.org/ 0000-0002-2064-4175

Rondón Contreras, Jairo: *Ph.D. in Applied Chemistry, mention Materials Study, 2015, Universidad de Los Andes; Professor of Biomedical & Chemical Engineering Departments, at the Polytechnic University of Puerto Rico, San Juan, PR-USA. Email: jrondon@pupr.edu*

https://orcid.org/0000-0002-9738-966X

Rodríguez Sulbarán, Pedro: *Doctor of Science in Chemistry, 2025, Universidad de Concepción, Chile; Ph.D. in Applied Chemistry, mention Materials Studies, 2015, Universidad de Los Andes; Professor of Chemistry Department (Kinetics and Catalysis Laboratory), at the Faculty of Sciences, ULA. Mérida, Venezuela. Correo electrónico: pedrojrs@gmail.com*

https://orcid.org/0000-0002-1309-8532